


Letter

Two-Code Keying and Code Conversion for Optical Buffer Design in Optical Packet Switching Networks

Kai-Sheng Chen ¹, Chien-Sheng Chen ^{2,*} and Xiao-Lu Wu ¹

¹ School of Electrical and Computer Engineering, Nanfang College of Sun Yat-Sen University, Guangzhou 510970, China; 17304@mail.nfu.edu.cn (K.-S.C.); wuxiaolu1025@foxmail.com (X.-L.W.)

² Department of Information Management, Tainan University of Technology, Tainan 71002, Taiwan

* Correspondence: t00243@mail.tut.edu.tw; Tel.: +886-6-2532106-283

Received: 27 September 2019; Accepted: 2 October 2019; Published: 3 October 2019



Abstract: Buffering management is a crucial function in current optical packet switching (OPS) networks. To avoid packet blocking due to competition for the same switched path, optical buffering is required to queue packets after a router makes the forwarding decision. In this paper, the author proposed a buffering scheme based on optical code-division multiple access (OCDMA), where each packet is encoded with an optical signature code. An optical coding technique combining spectral-amplitude coding (SAC) and two-code keying (TCK) is introduced to advance the buffering performance regarding packet loss probability. In TCK, the payload bits “1” and “0” of a stored packet are respectively converted to a SAC signal and its complementarity. As the Hamming distance between the coding signals of bits “1” and “0” is extended, the existing drawback that the OCDMA-based buffer capacity is limited by the decoder noise increased with the number of queued SAC packets is resolved. Moreover, an encoder consisting of a fiber Bragg grating (FBG) array is applied for simplifying the system design. A SAC signal and its complementary counterpart can be generated simultaneously without the need of an extra encoder.

Keywords: optical switching network (OPS); optical code-division multiple access (OCDMA); spectral-amplitude coding (SAC); two-code keying (TCK); optical buffer

1. Introduction

Optical packet switching (OPS) is a primary technique to realize all-optical networks with sufficient data capacity [1–3]. However, the limitation of OPS deployment exists due to packet-storage issues. Two or more packets face a contention when a router in the network tries to forward them to the same output port. Contention resolution and packet buffering should be performed while the packets are being routed. Electrical buffering schemes, such as random access memory (RAM), have yet to be maturely implemented in the optical domain [4,5]. Optical memory is proposed to avoid signal collision and increase switching efficiency [6–12]. There are three primary methods: time-domain contention resolution [6–8], wavelength routing [9–11], and code conversion [12,13].

Fiber delay lines (FDLs) act as memory units with an algorithm of first-in-first-out (FIFO) in OPS networks [6–8]. An FDL is a section of fiber with a fixed length made up of several loops. The delay from the traveling time of passing through an FDL buffer is used to protect the packet from the congestion of others in the same time slot. Optical buffering can also be implemented in the wavelength domain [9–11]. A tunable wavelength converter (TWC) transforms the wavelength of the incoming packet into a new one selected from the available wavelength set. Packets with various wavelengths are kept in a shared memory device without being spread over multiple time slots.

With the emergence of optical code-division multiple access (OCDMA) in data transmissions, code conversion is launched to solve the contention problem without delaying the packets [12,13].

It is usually operated by an optical cross-connect (OXC) in the network router so that it has a similar buffering function of a memory device. Since codec complexity has been reduced recently, code conversion is now more commonly applied to buffering management to increase the information rate in OPS. Every payload bit in a packet is referred to as a signature code in the time, wavelength, or space domain. The buffer extracts the code information from the input packet and substitutes the previous code with a new one.

The performance of an OCDMA system is limited by multiple access interference (MAI) [14] or the noise terms raised during the process of optical-to-electrical conversion at the decoders [15–18]. To enhance buffering performance by accommodating more queued signals, a hybrid scheme that switches both code and wavelength of packets, known as wavelength-division multiplexing (WDM)/OCDMA, is proposed in [12]. Although WDM/OCDMA expands the dimension of packet storage from the code to the wavelength domain, other light spectrum is required, and bandwidth usage is reduced. Alternatively, one can decrease the probability of packet loss due to the incorrect decoding of the OCDMA packets by encoding them with optical codes with very low in-phase cross-correlation values [17]. However, the types and the numbers of such codes are limited, and the power usage of light sources is not efficient as many power components are blocked when the code-words with relatively more chip “0s” are generated.

In this paper, we adopt the coding scheme of two-code keying (TCK) to fit the code conversion design in the optical buffer. TCK encodes distinct codes on the optical spectrum according to the values of data bits [15,16,18]. This scheme was initially used in optical access networks to enhance communication security and increase the system signal-to-noise ratio (SNR). When TCK is used for the buffer design, a larger capacity is expected due to the increased number of multiplexed packet signals that can be correctly decoded under a designated noise level. The coding technique of spectral-amplitude coding (SAC) [15–18] is employed to reduce the buffer complexity, where the coded and the complementary coded signals can be generated from a single encoder.

The rest of this paper is organized as follows. In Section 2, typical buffering schemes, including FDL and OCDMA buffers, are reviewed, and the coding technique of TCK in the OCDMA buffer is introduced. In Section 3, the author describes the buffer architecture that supports optical packet buffering based on TCK and code conversion, and the variations of packet signals during the buffering processes are demonstrated. In Section 4, the modeling of the proposed buffer is conducted to derive performance measures. Finally, Section 5 gives a conclusion.

2. Optical Buffering with Two-Code Keying (TCK) and Code Conversion

In this section, we introduce the fundamental characteristics of the proposed OCDMA-based buffer and compare them with those of conventional FDL. Figure 1a shows an $N \times 1$ FDL buffer where N input packets are competing for a common output path. The buffer arranges packets in non-overlapping time slots to avoid signal collisions. Each FDL queues a packet with a delay of nD , where D is the unit delay time, and n is a positive integer of the loop number of the FDL. To effectively schedule the packet leaving, a control unit in the buffer assigns a suitable delay to each packet according to its arrival time and length. Contention resolution is performed as all N delayed packets can be multiplexed in a single output channel without interference. In this scheme, packets cannot be stored contiguously in time as each FDL only provides a discrete delay. Interruptions between packets result in that the buffer length is longer than the length summation of the original packets. When all FDLs are occupied, new arriving packets are discarded.

The scheme in Figure 1b shows the structure of an N -input single-output optical buffer based on optical encoding that expresses each packet as an OCDMA signal. The reason for encoding packets is to avoid drops resulting from signal collisions. For optical buffering, packets P_1, P_2, \dots, P_N are encoded with optical codes C_1, C_2, \dots, C_N , respectively. In this scheme, one packet may partially overlap with another. By employing appropriate detection methods and the orthogonal property among OCDMA codes, the desired packet can be decoded from the packet stack without interference. As packets are

stored in the code dimension, they are not delayed or slowed, and the only waiting time comes from the encoding processes. Therefore, the OCDMA buffer has better efficiency in terms of time utilization than FDL.

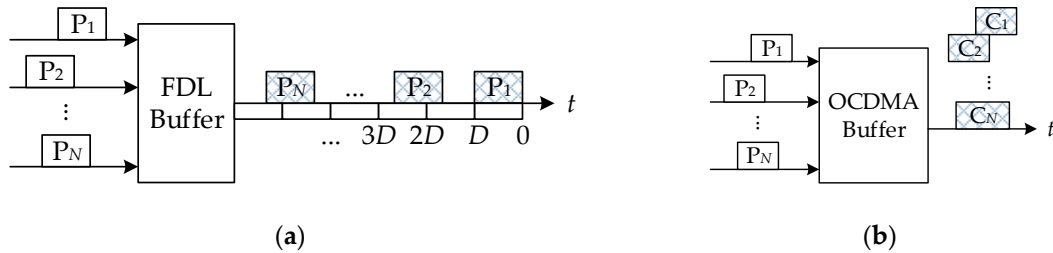


Figure 1. Optical buffering scheme based on (a) fiber delay line (FDL) and (b) optical code-division multiple access (OCDMA).

In this paper, we proposed an OCDMA-based buffer combined with TCK. By converting the packet payload into an optical code and its complement, the packet signal is more robust in the noise-dominant environment. The buffer capacity is increased as more packets can be stored under a given noise level. For an OCDMA buffering scheme of on-off keying (OOK), bit “1” is presented as an optically coded signal while for a bit “0”, the optical power is absent, as shown in Figure 2a. If TCK is adopted, an additional signal of complementary code is used to convey bit “0s” in the packet. During the whole packet interval, the optical power for the packet does not vary with the bit values and remains nearly constant, as shown in Figure 2b. In this figure, \bar{C}_k denotes the complementary code of C_k , where $1 \leq k \leq N$.

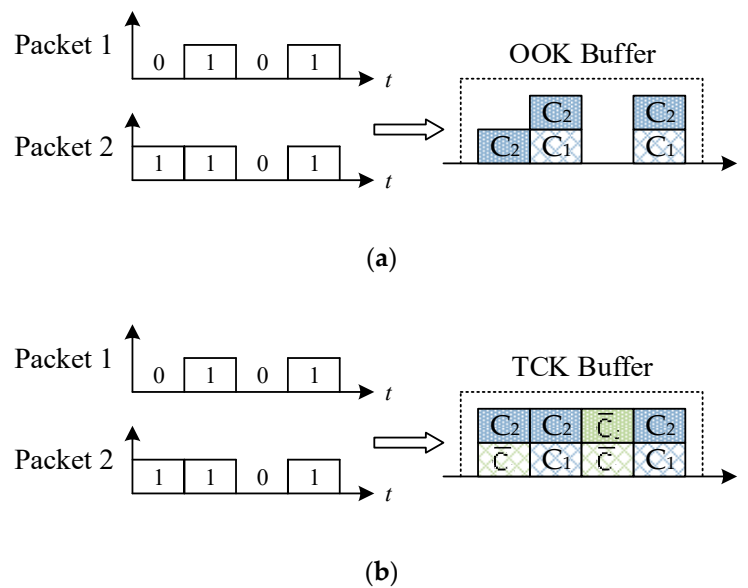


Figure 2. Optical coding scheme for buffered packets: (a) on-off keying (OOK) and (b) two-code keying (TCK).

As each buffered packet is assigned with a specific code, the orthogonal property among OCDMA signals can be employed to distinguish the desired signal from the packet stack. SAC was initially proposed in optical access networks to achieve asynchronous and simultaneous transmissions without multiple-access interference (MAI). This author introduces SAC as a possible method to cancel the interference resulting from the overlapping packets in the buffer. Several TCK systems in SAC, such as residue-stuffed QC (RSQC) codes [16] and Walsh–Hadamard codes [18] have been proposed to

provide a 3-dB gain in the SNR to reduce the signal errors. Considering the buffer design of TCK of Walsh–Hadamard codes, the MAI effect can be cancelled by executing the following algorithms [18]:

$$C_k \odot C_j - \bar{C}_k \odot C_j = \begin{cases} N/2, & k = j \\ 0, & k \neq j \end{cases} \quad (1)$$

$$\bar{C}_k \odot C_j - \bar{C}_k \odot \bar{C}_j = \begin{cases} -N/2, & k = j \\ 0, & k \neq j \end{cases} \quad (2)$$

where N is the code length and \odot is the symbol of the dot-product. To decode the packet of C_k or \bar{C}_k , the receiver generates an exactly identical local code and performs the correlation function of (1) or (2), respectively.

3. System Configuration

A single-input single-output OCDMA buffer with capacity K consisting of parallel encoders/decoders and optical cross-connects (OXC) is shown in Figure 3. The main idea is to express several buffered packets as the multiplexed SAC signals overlapped in the time domain. Decoders at the buffer input detect the coded and the complementary coded signals from the payload bits “1” and “0” of the incoming packet. After one of the available codes that are not occupied by other buffered packets is selected, the switch control unit (SCU) establishes a link configuration in the $1 \times K$ OXC to forward the optical carrier generated from a broadband light source (BLS) to the corresponding encoder. Then a 1×2 OXC determines the output signal from a code set consisting of the typical and the complementary codes based on the values of electrical payload bits. Finally, packet buffering is achieved by performing code conversion on the incoming packet. In this figure, $d_i^{(1)}$ and $d_i^{(0)}$ denote the coded signals for encoding payload bit “1” and “0” from decoder i , respectively, where $1 \leq i \leq K$.

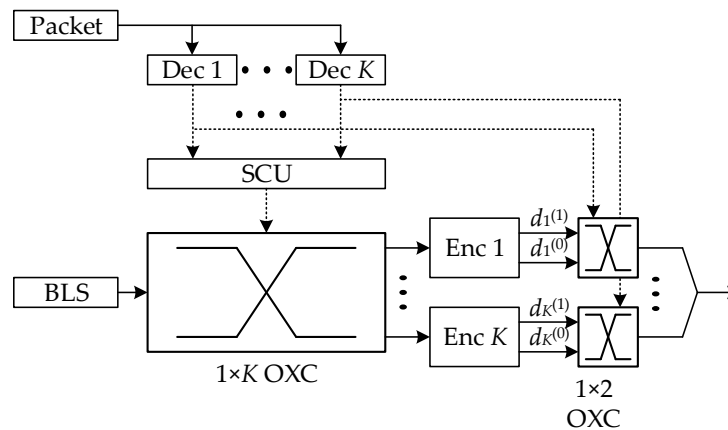


Figure 3. OCDMA buffer architecture with code conversion and TCK. BLS: broadband light source; Enc: encoder; Dec: decoder; EOM: electrical-to-optical modulator; SCU: switch control unit.

The codec in Figure 4 is designated to be capable of generating and detecting Walsh–Hadamard codes. These codes can be found in the rows of Hadamard matrices, which were introduced by Jacques Hadamard in 1893 [19]. The matrix H_n has the elements of $\{1, -1\}$ and the order of 1, 2, and $4n$, where n is a positive integer. Two Hadamard matrices with the same order n have the property of $H_n H_n^T = nI_n$, where I_n is the identity matrix of order n . As the optical power is unipolar, the entries of H_n are

modified into 1s and 0s to fit for optical coding. Given that $n = 4$, the relationships between Hadamard matrices and the code vectors used for TCK are given as:

$$H_4 = \begin{bmatrix} 1 & 1 & 1 & 1 \\ 1 & 0 & 1 & 0 \\ 1 & 1 & 0 & 0 \\ 1 & 0 & 0 & 1 \end{bmatrix} = \begin{bmatrix} 1 & 1 & 1 & 1 \\ C_1 & & & \\ C_2 & & & \\ C_3 & & & \end{bmatrix} \quad (3)$$

$$\bar{H}_4 = \begin{bmatrix} 0 & 0 & 0 & 0 \\ 0 & 1 & 0 & 1 \\ 0 & 0 & 1 & 1 \\ 0 & 1 & 1 & 0 \end{bmatrix} = \begin{bmatrix} 0 & 0 & 0 & 0 \\ \bar{C}_1 & & & \\ \bar{C}_2 & & & \\ \bar{C}_3 & & & \end{bmatrix} \quad (4)$$

where \bar{H}_n is a matrix with each element being 2's complement of H_n 's elements. For a Hadamard matrix with order $m = 4n$, at most $(m - 1)$ codes are available, as the receiver cannot reject the MAI resulting from the codes of all zeros and all ones.

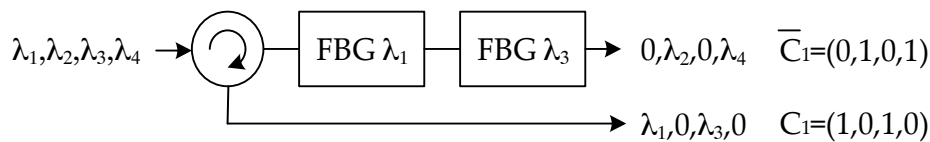


Figure 4. Encoder structure of Hadamard codes with code length $N = 4$. FBG: fiber Bragg grating.

An encoder consisting of fiber Bragg gratings (FBGs) is employed to generate SAC signals for packet buffering. Figure 5 shows the encoder structure of Hadamard code $C_1 = (1, 0, 1, 0)$ and $\bar{C}_1 = (0, 1, 0, 1)$. As the code chip is encoded on the spectrum, the signal wavelengths corresponding to C_1 are $(\lambda_1, 0, \lambda_3, 0)$. These two wavelengths are thrown back by the two FBGs with reflection wavelengths λ_1 and λ_3 , respectively. The passed wavelengths, λ_2 and λ_4 , form the wavelength assignment of $(0, \lambda_2, 0, \lambda_4)$, which exactly matches the chip distribution of \bar{C}_1 .

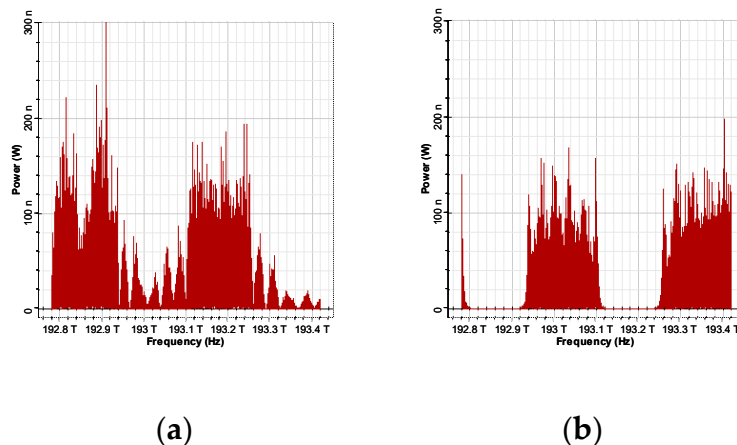


Figure 5. The coded packet signals in the wavelength domain (a) Hadamard code $(1, 0, 1, 0)$; and (b) complementary Hadamard code $(0, 1, 0, 1)$.

In SAC, the encoding process that avoids packet loss due to the collision is performed in the wavelength domain, so the patterns of optical codes cannot be observed in the time waveforms of packets, which are only determined by the payload sequences. The power spectral density (PSD) of the signal of a Hadamard code C_k with length N is composed of $N / 2$ wavelengths filtered from a BLS spectrum by an FBG array. The remaining wavelengths not filtered by FBGs are used to modulate the

packet assigned with complementary code \bar{C}_k . Figure 5a,b shows the coded signals of Hadamard codes of $C_1 = (1,0,1,0)$ and $\bar{C}_1 = (0,1,0,1)$ in the wavelength domain, respectively. Figure 6a–c shows the time waveforms of electrical payload sequence, the optically coded packet of TCK, and the demodulated payload sequence. Note that as payload bits “1” and “0” were both encoded with SAC codes with equal power, so they had similar amplitudes, and the payload values could not be identified in Figure 6b. Furthermore, comparing Figure 6a with Figure 6c, one can find that the payload sequences had become bi-polar as the decoded results of bit “1s” and “0s” from the correlation algorithms of (1) and (2) were inverse numbers. The simulations were conducted using the Optisystem 7.0 software. The power, bandwidth, and center wavelength of the BLS are -10 dBm, 3.75 THz, and 193.1 THz, respectively. The packets were assumed to have a bit rate of 10 Gb/s. The FBGs had a bandwidth of 0.9375 THz, reflection wavelengths of 191.71 THz and 193.57 THz, and reflectivity of 0.9998 .

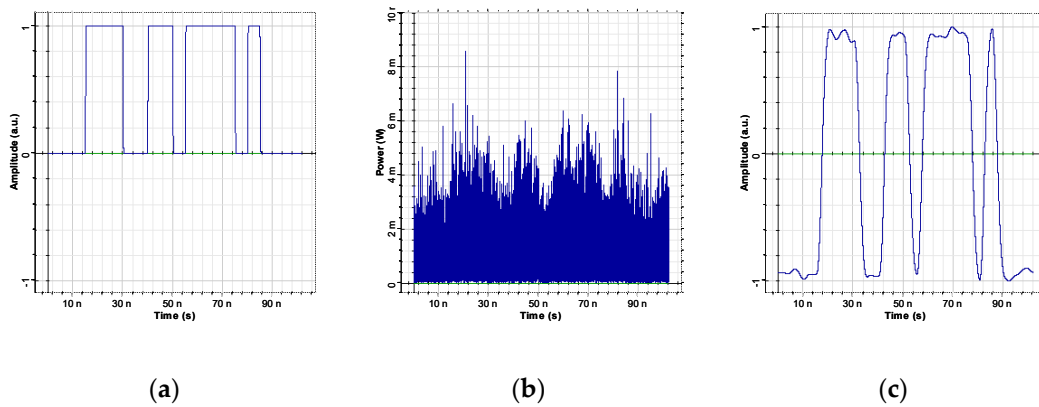


Figure 6. Time waveforms of (a) electrical payload sequence before optical modulation; (b) optical coded packets with TCK; and (c) demodulated payload sequence.

4. Buffering Performance Analysis

In this section, we analyze the performance of the proposed buffer system. Effects of incoherent intensity noise and thermal noise in the photo-detectors for demodulating optical packets were investigated. The Gaussian approximation was proposed for quantifying the performance index of bit-error rate (BER). The variance of photo-current comes from the occurrence of spontaneous emission when a light signal is detected, which can be expressed as

$$\langle i^2 \rangle = \left(S_{TH} + R^2 \int_0^\infty G^2(v) dv \right) B \quad (5)$$

In (5), the first term denotes the thermal noise and the second is the variance of phase-intensity induced noise (PIIN) [19], where S_{TH} is the PSD of thermal noise, R is the responsiveness of the photodiode, and B is the electrical-equivalent noise bandwidth. $G(v)$ is the PSD of the stacked packets in the buffer, which can be written as

$$G(v) = \frac{P_{sr}}{\Delta v} \sum_{k=1}^K \sum_{i=1}^N c_k(i) \prod \left[\frac{N}{\Delta v} \left(v - v_0 + \frac{1}{2N} \right) - \left(i + \frac{1}{2} \right) \right] \quad (6)$$

where P_{sr} is the effective power of light source at the receiver, K is the packet number in the buffer, Δv is the optical source bandwidth, and $c(i)$ is the i -th element of Hadamard code C_i . $\prod(v)$ denotes a unit-width rectangular function centered at 0. As the correlation properties for Hadamard codes and their complements are similar, to simplify the analysis, we assumed that the payload sequences

for K packets in the buffer were all bits “1”. Based on the assumptions on the light source in [19], the mathematical expression for the integral in (5) can be expressed as

$$\int_0^\infty G^2(v)dv = \frac{P_{sr}^2}{4\Delta v} K(K+1) \quad (7)$$

Then BER can be derived by using the following expression:

$$P_e = \frac{1}{2} \operatorname{erfc} \left[\frac{RP_{sr}N/2}{\sqrt{2BS_{th} + BR^2P_{sr}^2K(K+1)/2\Delta v}} \right] \quad (8)$$

The numerator term in (8) represents the photo-current of decoding a Hadamard-coded packet.

Figure 7 shows the BER as a function of light source power P_{sr} . The parameters used for analysis were $S_{TH} = 1.6 \times 10^{-22}$ W/Hz, $R = 0.95$ A/W, $B = 1$ GHz, and $\Delta v = 0.6$ THz and others were the same as the ones used in Figures 5 and 6. When P_{sr} was relatively small, the BERs for OOK and TCK were close. When P_{sr} increased, the proposed scheme had a lower BER, due to the larger power of photo-current achieved by encoding SAC codes on both bits “1” and “0”. The BER improvement for the OOK buffer was less efficient, as the increment of photo-current was not enough to get a significantly high signal-to-noise ratio (SNR). Furthermore, the comparison between the numerical analysis and simulations were shown in this figure. Instead of using the mathematical deductions, we used electrical power meters to measure the signal powers at photo-detectors to obtain the photo-current and the PIIN power for simulation. It can be observed that the BER values from these two methods had close results, which indicated the rigidity of the used scheme for performance analysis.

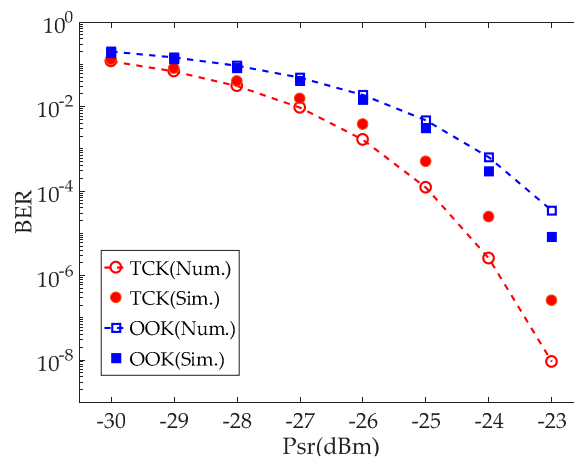


Figure 7. Bit-error rate (BER) versus the effective power of light source P_{sr} for an OOK and TCK packet. Num.: numerical analysis; Sim.: simulation.

The improved BER results achieved by employing TCK for optical buffering were further supported by Figure 8. Two eye diagrams were presented at the light source power $P_{sr} = -22$ dBm for a single packet of TCK and OOK. It revealed that the eye height in Figure 8a was higher than that in Figure 8b, and the patterns were clearer. This indicated that the proposed buffer scheme had enhanced performances, despite the presence of noise sources.

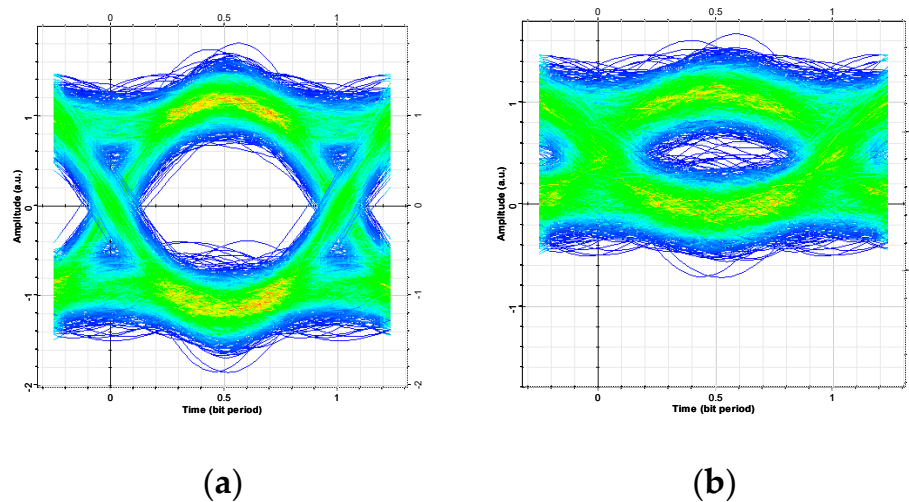


Figure 8. Eye diagrams of payload signals in (a) TCK and; (b) OOK buffers.

In Figure 9, BERs of the conventional OOK and TCK buffers were analyzed under different multiplexed packet numbers. The increase of K resulted in the increase of optical power detected at photo-detectors, which induced a more considerable noise variance. As one could anticipate, TCK buffer had increased capacity at a given BER. Despite the presence of photo-current variations, the decoder had a higher probability of correctly identifying the packet payloads due to the large Hamming distance between signals “1” and “0” achieved by employing TCK.

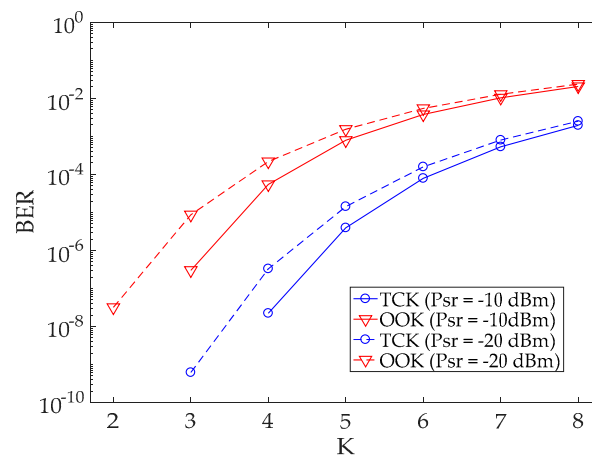


Figure 9. BER versus buffer capacity K .

In Figure 10, one can observe the buffer capacity versus various electrical bandwidths at $\text{BER} = 10^{-9}$. A system with a larger bandwidth is capable of supporting higher packet rates. However, the noise power is proportional to the receiver bandwidth, so there is a tradeoff between packet rates and BER. This limitation could be partially relieved by employing the TCK buffer, which can store more packets than the OOK one, for a designated BER.

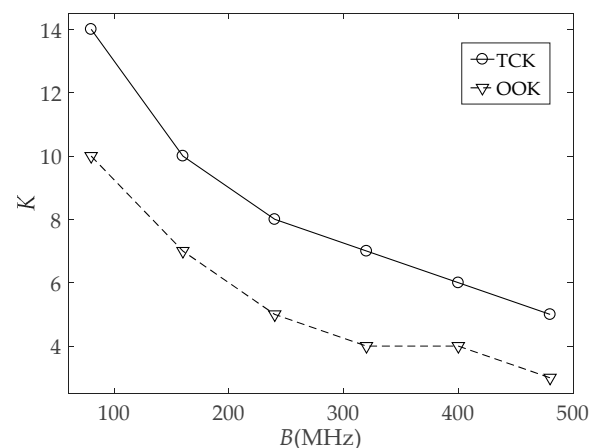


Figure 10. Buffer capacity K versus receiver bandwidth B .

5. Conclusions

The application of TCK in an OCDMA-based buffer in OPS networks was investigated in this paper. The number of queued packets in the proposed buffer was increased by assigning packets with OCDMA signals and their complementary codes. The buffering performances in BER and buffer capacity were obtained by numerical analysis and simulations by considering the thermal noise and PIIN. The proposed TCK buffer could lead to a reduction of the BER as the Hamming distance between payload bits “1” and “0” is twice than that of the OOK buffer, which obtains a larger SNR. Moreover, the author found a cost-effective encoder based on FBGs that simultaneously generates an OCDMA signal and its complementary counterpart. For future works, the authors aim to adopt channel coding in OPS as a solution to resolve packet contention, prevent packet loss, as well as enhance network security [20]. Except for simply considering the capacity, investigating other physical constraints in OPS such as survivability, secrecy, and processing would give more adequate insights for optical buffer systems.

Author Contributions: K.-S.C. contributed to the conceptualization, methodology, and writing of this paper. C.-S.C. conducted the investigation and contributed to writing—review & editing. X.-L.W. conceived the simulation setup and formal analysis.

Funding: This research was funded by Department of Education of Guangdong Province, grant number 2018K TSCX322.

Conflicts of Interest: The authors declare no conflict of interest.

References

- Segawa, T.; Ibrahim, S.; Nakahara, T.; Muranaka, Y.; Takahashi, R. Low-power optical packet switching for 100-Gb/s burst optical packets with a label processor and 8×8 optical switch. *J. Lightwave Technol.* **2016**, *34*, 1844–1850. [\[CrossRef\]](#)
- Zhao, Z.; Wu, B.; Li, B.; Xiao, J.; Fu, S.; Liu, D. Multihop Routing Enabled Packet Switching With QoS Guarantee in Optical Clos for Data Centers. *J. Opt. Commun. Netw.* **2018**, *10*, 624–632. [\[CrossRef\]](#)
- Argibay-Losada, P.J.; Yoshida, Y.; Maruta, A.; Schlosser, M.; Kitayama, K. Performance of fixed-length, variable-capacity packets in optical packet-switching networks. *IEEE/OSA J. Opt. Commun. Netw.* **2015**, *7*, 609–617. [\[CrossRef\]](#)
- Koyano, S.; Ata, S.; Iwamoto, H.; Yano, Y.; Kuroda, Y.; Inoue, K.; Oka, I. A study on micro level traffic prediction for energy-aware routers. *ACM SIGOPS Oper. Syst. Rev.* **2013**, *47*, 26–33. [\[CrossRef\]](#)
- Iwamoto, H.; Yano, Y.; Kuroda, Y.; Yamamoto, K.; Ata, S.; Inoue, K. Deterministic Packet Buffer System with Multi FIFO Queues for the Advanced QoS. *IEICE Trans. Commun.* **2013**, *96*, 1819–1825. [\[CrossRef\]](#)
- Datta, A. Construction of polynomial-size optical priority queues using linear switches and fiber delay lines. *IEEE/ACM Trans. Netw.* **2017**, *25*, 974–987. [\[CrossRef\]](#)

7. Lim, H. Number of tunable wavelength converters and internal wavelengths needed for cost-effective design of asynchronous optical packet switching system with shared or output fibre delay line buffer. *IET Commun.* **2013**, *7*, 1419–1429. [[CrossRef](#)]
8. Wang, X.; Jiang, X.; Pattavina, A. Constructing N-to-N Shared Optical Queues with Switches and Fiber Delay Lines. *IEEE Trans. Inf. Theory* **2012**, *58*, 3836–3842. [[CrossRef](#)]
9. Liu, W.; Romeira, B.; Li, M.; Guzzon, R.S.; Norberg, E.J.; Parker, J.S.; Coldren, L.A.; Yao, J. A Wavelength Tunable Optical Buffer Based on Self-Pulsation in an Active Microring Resonator. *J. Light. Technol.* **2016**, *34*, 3466–3472. [[CrossRef](#)]
10. Miyazawa, T.; Hirayama, T.; Furukawa, H.; Harai, H. Optical and Electronic Combined Buffer Architecture for Optical Packet Switches. *J. Opt. Commun. Netw.* **2015**, *7*, 776–784.
11. Liu, L.; Zhang, Z.; Yang, Y. In-Order Packet Scheduling in Optical Switch With Wavelength Division Multiplexing and Electronic Buffer. *IEEE Trans. Commun.* **2014**, *62*, 1983–1994. [[CrossRef](#)]
12. Kazemi, R.; Rashidinejad, A.; Nashtaali, D.; Salehi, J.A. Virtual Optical Buffers: A Novel Interpretation of OCDMA in Packet Switch Networks. *J. Light. Technol.* **2012**, *30*, 2964–2975. [[CrossRef](#)]
13. Liu, C.-C.; Chang, Y.-T.; Yang, C.-C.; Huang, J.-F. Packets Buffering Enhancement with Hybrid Coding Labels for Virtual Optical Memory. *Procedia Comput. Sci.* **2018**, *130*, 336–343. [[CrossRef](#)]
14. Cai, Y.; De Lamare, R.C.; Fa, R. Switched Interleaving Techniques with Limited Feedback for Interference Mitigation in DS-CDMA Systems. *IEEE Trans. Commun.* **2011**, *59*, 1946–1956. [[CrossRef](#)]
15. Yang, C.-C. Code Space Enlargement for Hybrid Fiber Radio and Baseband OCDMA PONs. *J. Light. Technol.* **2011**, *29*, 1394–1400. [[CrossRef](#)]
16. Yang, C.-C.; Huang, J.-F.; Chang, H.-H.; Chen, K.-S. Radio Transmissions over Residue-Stuffed-QC-Coded Optical CDMA Network. *IEEE Commun. Lett.* **2013**, *18*, 329–331. [[CrossRef](#)]
17. Chen, K.-S.; Yang, C.-C.; Huang, J.-F.; Cheng, K.-S. Using Stuffed Quadratic Congruence Codes for SAC Labels in Optical Packet Switching Network. *IEEE Commun. Lett.* **2015**, *19*, 1093–1096. [[CrossRef](#)]
18. Huang, J.-F.; Yang, C.-C.; Tseng, S.-P. Complementary Walsh–Hadamard coded optical CDMA coder/decoders structured over arrayed-waveguide grating routers. *Opt. commun.* **2014**, *229*, 241–248. [[CrossRef](#)]
19. Wei, Z.; Shalaby, H.; Ghafouri-Shiraz, H. Modified quadratic congruence codes for fiber Bragg-grating-based spectral-amplitude-coding optical CDMA systems. *J. Light. Technol.* **2001**, *19*, 1274–1281.
20. Kravetska, K.; Overby, H.; Gligoroski, D. Coded Packet Transport for Optical Packet/Burst Switched Networks. In Proceedings of the 2015 IEEE Global Communications Conference (GLOBECOM), San Diego, CA, USA, 6–10 December 2015; pp. 1–6.



© 2019 by the authors. Licensee MDPI, Basel, Switzerland. This article is an open access article distributed under the terms and conditions of the Creative Commons Attribution (CC BY) license (<http://creativecommons.org/licenses/by/4.0/>).